DNA: REPLICATION REPAIR AND RECOMBINATION:

Functional Oligomeric State of Avian Sarcoma Virus Integrase

Kogan K. Bao, Hong Wang, Jamie K. Miller, Dorothy A. Erie, Anna Marie Skalka and Isaac Wong

J. Biol. Chem. 2003, 278:1323-1327.
doi: 10.1074/jbc.C200550200 originally published online November 21, 2002

THE JOURNAL OF BIOLOGICAL CHEMISTRY
Vol. 278, No. 2, Issue of January 10, pp. 1323–1327, 2003
Printed in U.S.A.

Functional Oligomeric State of Avian Sarcoma Virus Integrase*

Received for publication, September 27, 2002, and in revised form, November 7, 2002
Published, JBC Papers in Press, November 21, 2002, DOI 10.1074/jbc.C200550200

Kogan K. Bao‡, Hong Wang§, Jamie K. Miller‡, Dorothy A. Erie§, Anna Marie Skalka¶, and Isaac Wong‡‖

From the ‡Department of Biochemistry and Biophysics, Oregon State University, Corvallis, Oregon 97331, the §Department of Chemistry, University of North Carolina at Chapel Hill, Chapel Hill, North Carolina 27599, and the ¶Institute for Cancer Research, Fox Chase Cancer Center, Philadelphia, Pennsylvania 19111

Retroviral integrase, one of only three enzymes encoded by the virus, catalyzes the essential step of inserting a DNA copy of the viral genome into the host during infection. Using the avian sarcoma virus integrase, we demonstrate that the enzyme functions as a tetramer. In presteady-state active site titrations, four integrase protomers were required for a single catalytic turnover. Volumetric determination of integrase-DNA complexes imaged by atomic force microscopy during the initial turnover additionally revealed substrate-induced assembly of a tetramer. These results suggest that tetramer formation may be a requisite step *during* catalysis with ramifications for antiviral design strategies targeting the structurally homologous human immunodeficiency virus, type 1 (HIV-1) integrase.

Integrase catalyzes two consecutive transesterification reactions during its *in vivo* function (1, 2). In the "processing" reaction, the reverse transcriptase-generated DNA copy of the viral genome is trimmed by the endonucleolytic removal of the 3′-dinucleotides from its ends. The two processed 3′-ends are then inserted into opposing strands of the host DNA in the "joining" reaction via a concerted cleavage-ligation reaction (3–6). Purified integrase catalyzes both reactions on synthetic oligodeoxynucleotide substrates containing viral DNA end sequences in the presence of either Mn^{2+} or Mg^{2+} as a cofactor (7–10). *In vitro*, integrase also catalyzes the apparent reversal of the joining reaction, the "disintegration" activity, on Y-shaped oligodeoxynucleotide substrates (11) as illustrated in Fig. 1. These Y-shaped substrates resemble products of integrase-catalyzed joining and contain a nick immediately 5′ of the joining site. The disintegration reaction effectively reverses joining by resealing the nick while concurrently displacing the inserted viral sequence. This reaction is routinely used to assay integrase *in vitro* (8, 12–14).

Numerous structures of integrase catalytic core-containing fragments determined from a variety of retroviral sources have all been dimeric (15–21). However, the two active sites of the subunits in these structures are outwardly oriented on opposite sides of the crystallographic dimers, too far apart (>50 Å) to be spanned by the requisite 5–6 bp stagger separating the two sites of concerted integration on the host DNA (20). Although several tetrameric models have been hypothesized based on comparisons with the structure of the homologous bacterial Tn5 transposase (20–22), the structure for neither a full-length integrase nor an integrase-DNA complex has been solved, and the quaternary structure of the catalytically active integrase enzyme remains unknown.

We have previously elucidated some mechanistic aspects of substrate specificity for the processing reaction of the avian sarcoma virus (ASV)[1] integrase by presteady-state kinetics (9, 10); however, we were unable to determine the reaction stoichiometry using a synapsed processing substrate due to substrate-induced aggregation, a problem common to retroviral integrases (23). Here, we report the use of a presteady-state disintegration assay that mitigated these aggregation problems, allowing us to determine the reaction stoichiometry by active site titrations. Volumetric analysis of integrase particles imaged by atomic force microscopy during the first turnover additionally establishes the quaternary structure of the functional unit. Our results will be discussed in the context of the hypothesized tetramer models.

EXPERIMENTAL PROCEDURES

DNA and Proteins—Oligodeoxyribonucleotides were synthesized by the Center for Gene Research and Biotechnology Central Services Laboratory (Oregon State University). Purification by denaturing PAGE, spectrophotometric determination of concentrations, and 5′-radiolabeling were as described previously (9). Integrase was overexpressed in *Escherichia coli* BL21(DE3), purified as described (9), and stored at −80 °C in 50 mM HEPES, pH 7.5, 500 mM NaCl, and 40% glycerol.

Presteady-state Assays and Product Analysis by Denaturing Acrylamide Gel Electrophoresis—Standard reactions were carried out at 37 °C in 20 mM Tris, pH 8.0, 10 mM Na-HEPES, pH 7.5, 4% glycerol, 10 mM 2-mercaptoethanol, 0.050 mg ml^{-1} acetylated bovine serum albumin, 250 or 400 mM NaCl, and with or without 5 mM $MnCl_2$. Preincubations were carried out in the absence of $MnCl_2$ for 30 min and the reaction subsequently initiated by the addition of 37 °C $MnCl_2$ to 5 mM. A complete range of preincubation times and temperatures were tested to ensure that equilibrium had been achieved. Gel analysis, image quantitation, and non-linear least squares fittings were performed according to Bao *et al.* (9, 10).

Imaging by Atomic Force Microscopy (AFM)—Imaging was performed with a Nanoscope IIIa instrument (Digital Instrument, Santa Barbara, CA) using the tapping mode in air. Nanosensor Pointprobe non-contact/tapping mode sensors with a nominal spring constant of 48 newton/m and resonance frequencies of 190 kHz were used for all images. The protein and DNA molecules were deposited onto freshly cleaved mica (Spruce Pine Mica Co., Spruce Pine, NC), immediately washed with deionized distilled water, and dried with a stream of N_2 (gas). Depositions of disintegration reactions during the first catalytic turnover were obtained by preincubating 4 μM integrase with 5 μM substrate DNA in 20 mM Tris, pH 8.0, 10 mM HEPES, pH 7.5, and 250 mM NaCl for a minimum of 30 min on ice, diluting the reaction to 64 nM integrase and 150 mM NaCl immediately prior to initiating the reaction

* This work was supported by National Institutes of Health Grant GM58771 (to I. W.). The costs of publication of this article were defrayed in part by the payment of page charges. This article must therefore be hereby marked "*advertisement*" in accordance with 18 U.S.C. Section 1734 solely to indicate this fact.

‖ To whom correspondence should be addressed: Dept. of Biochemistry and Biophysics, Oregon State University, 2011 ALS Bldg., Corvallis, OR 97331. E-mail: wongis@onid.orst.edu.

[1] The abbreviations used are: ASV, avian sarcoma virus; AFM, atomic force microscopy; HIV-1, human immunodeficiency virus, type 1; IN, integrase.

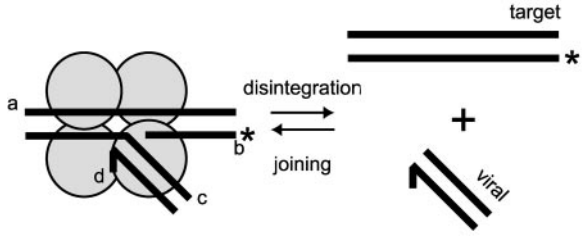

FIG. 1. **Schematic depicts integrase-catalyzed disintegration and joining reactions of the Y-substrate superimposed on a generic tetramer model for integrase (*left*).** The sequences of the component single-stranded synthetic oligonucleotides are: 5′-gcttgttgaataccatctaatcgtgtcgggtctcgtactgcggaa (*a*), ttccgcagtacgagacccg (*b*), aatgtagtcttatgcaatagc (*c*), and gctattgcataagactacaacacgattagatggtattcaacagc (*d*). The *asterisk* denotes the position of the 5′-^{32}P-radiolabel.

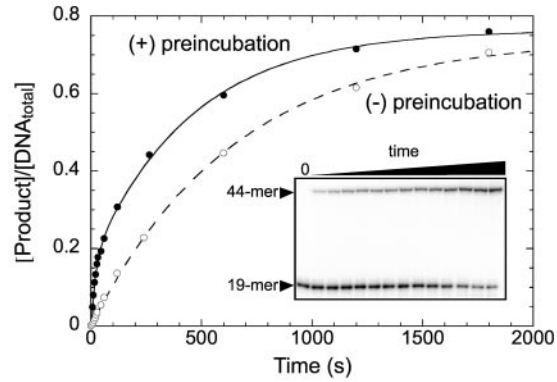

FIGS. 2. **Single-turnover time course of the disintegration reaction at 1 μM integrase and 0.25 μM substrate DNA was obtained by quantifying the amount of 44-mer formed following separation by denaturing PAGE (*inset*).** Experiments were conducted with (*closed circles*) and without (*open circles*) preincubating enzyme and substrate prior to initiating the reaction. *Lines* represent the best fit of the data to sum of exponential terms with $A_{1,\,preinc} = 0.17 \pm 0.01$, $A_{2,\,preinc} = 0.60 \pm 0.01$, $\lambda_{1,\,preinc} = 0.05\ s^{-1} \pm 0.006$, $\lambda_{2,\,preinc} = 0.002\ s^{-1} \pm 0.0001$, $A_{nonpreinc} = 0.74 \pm 0.009$, and $\lambda_{nonpreinc} = 0.002\ s^{-1} \pm 0.00004$.

by the addition of $MnCl_2$ to 5 mM. Aliquots were then deposited within 10 s of initiating the reaction. All images were collected with a scan rate of 3.2 Hz, at 512 × 512 resolution, and a scan size of 1 μm^2. Volume analysis of AFM data was performed with the freeware program ImageSXM (based on NIH Image developed at the National Institutes of Health) using image plane fitting, image analysis, volume calculations, and conversion to molecular weights according to MW_{app} = (volume x nm^{-3} + 25) ÷ 1.31 kDa^{-1} as described (24, 25).

RESULTS AND DISCUSSION

Single-turnover Disintegration Assays—For single-turnover experiments, the substrate was 5′-radiolabeled on the 19-nt target fragment, denoted by the *asterisk* in Fig. 1, which is converted to a 44-nt product during disintegration (*inset*, Fig. 2). Substrate (0.25 μM) was preincubated with excess ASV integrase (1 μM monomers) for 30 min in the absence of Mn^{2+} to allow equilibrium formation of productive complexes (9, 10). Reactions were initiated by the addition of Mn^{2+} to 5 mM. Fig. 2 (*closed circles*) shows biphasic conversion of the radiolabeled 19-nt substrate to the expected 44-nt product. Non-linear least squares fit of the data to a double-exponential function yielded observed rate constants of 0.05 and 0.002 s^{-1} with respective amplitudes of 17 and 60%. When the reaction was initiated by mixing integrase and substrate without preincubation but in the presence of Mn^{2+}, we observed a single 0.002 s^{-1} exponential phase (Fig. 2, *open circles*) with an amplitude (75 ± 0.9%) that was, within error, equal to the sum of the amplitudes (77 ± 1.4%) observed with preincubation. The fast phase reflected 17% productive integrase-substrate complexes formed during the preincubation period in the absence of Mn^{2+} that was rapidly converted to product at 0.05 s^{-1} upon addition of the metal cofactor. In contrast, the 0.002 s^{-1} phase observed in both experiments reflected slower assembly of productive complexes in the presence of Mn^{2+}. The significant amplitude of the slower exponential phase in the preincubated experiment, therefore, indicated that 60% more productive complexes were formed following the addition of the metal cofactor, suggesting that the formation of these complexes is facilitated by the presence of the metal cofactor (26).

Active Site Titrations—When experiments were performed at lower concentrations of integrase with preincubation, the amplitudes of the two exponential phases became reduced and an additional linear phase became apparent (Fig. 3*A*, *inset*). The apparent "burst" kinetics behavior is characteristic of enzymatic mechanisms where products are formed at the active site faster than they dissociate, resulting in rapid turnover of the first equivalent of substrates bound while subsequent steady-state turnovers are rate-limited by slow product release to regenerate the free enzyme. As in the single-turnover experiments, the first turnover burst consisted of two exponential phases reflecting the rapid 0.05 s^{-1} conversion of productive complexes preformed in the absence of Mn^{2+} followed by a slower rate of assembling additional complexes in the presence of the Mn^{2+}.

To determine the number of integrase protomers required to catalyze the disintegration of a single substrate, we performed active site titrations by measuring the sum of the two exponential amplitudes at fixed DNA concentrations as a function of increasing integrase to substrate DNA ratio. Fig. 3*A* shows two such titrations carried out at 250 mM NaCl with 0.25 μM DNA and at 400 mM NaCl with 0.5 μM DNA. In both cases, the total first turnover amplitude increased linearly with added integrase up to a ratio of four integrase protomers per substrate DNA. At integrase:substrate ratios above 4:1, a plateau was reached with no further apparent change in the burst amplitude, indicating that the substrate binding capacity of the added integrase exceeded the concentration of substrate. These results defined a reaction stoichiometry of four protomers per substrate molecule. Additionally, the same reaction stoichiometry was obtained at different DNA and NaCl concentrations, and titrations performed using integrase purified by different protocols also yielded identical results (data not shown).

The maximum burst amplitude observed at both salt concentrations represented less than complete binding of substrate DNA added albeit to different extents. If the missing 15–25% reflected a subpopulation of substrate that could not be bound by integrase, then the measured reaction stoichiometry of four should be divided by this plateau value to obtain the true reaction stoichiometry. On the other hand, if the missing fraction represented a subpopulation of integrase-substrate complex that was silent in the disintegration assay, *i.e.* did not generate the monitored product, then an adjustment may not be necessary. When we monitored the release of the viral-end fragment from the Y-shaped substrate rather than the regeneration of the 44-nt target fragment under identical conditions, we observed an additional exponential phase in which the missing 15–25% of the substrate was slowly cleaved (2×10^{-5} s^{-1}) to completion at the viral-target joining junction (data shown in Fig. 3*B* for 250 mM NaCl). This reaction was integrase-catalyzed yet could not have arisen from 3′-hydroxyl attack by the target 19-nt fragment as the corresponding target 44-mer product was not generated concurrently. We therefore concluded that the missing 15–25% amplitude represented a competing but silent subpopulation of the *integrase-substrate complex* that underwent hydrolytic attack at the joining junc-

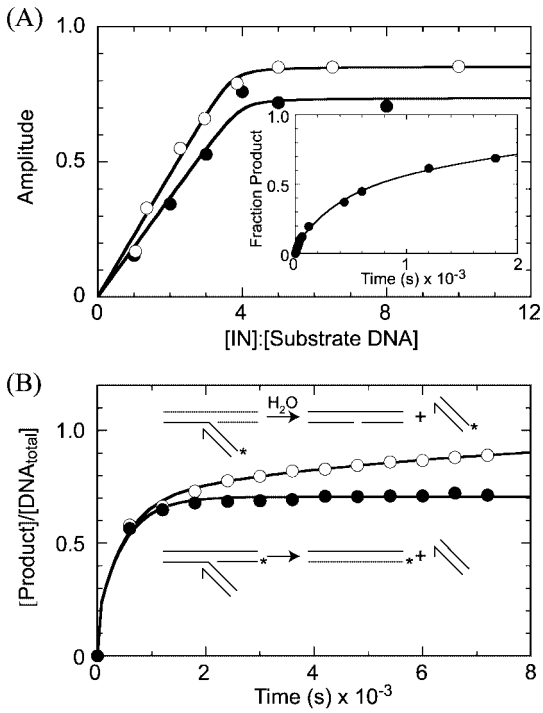

FIG. 3. *A*, disintegration reactions performed using less than 4-fold molar excess of integrase over substrate DNA showed burst kinetics as shown in inset for 0.25 μM DNA and 0.5 μM integrase at 250 mM NaCl. Best fit of the data to a double-exponential plus a line yielded a total burst amplitude of 0.4. Active site titrations for 0.25 μM DNA with 250 mM NaCl (*closed circles*) and 0.5 μM DNA with 400 mM NaCl (*open circles*) plotting the total burst amplitude as a function of the molar ratio of integrase monomer to substrate DNA show that saturation is reached at a four to one reaction stoichiometry. Best fits of the data (*solids lines*) to the following equation,

$$y = 0.5A_{max}[DNA]^{-1}(K_d + \alpha^{-1}[IN] + [DNA] - \sqrt{K_d + \alpha^{-1}[IN] + [DNA] - 4\alpha^{-1}[IN][DNA]}) \quad \text{(Eq. 1)}$$

using an arbitrarily fixed $K_d < 1$ nM yielded maximum amplitudes, A_{max}, of 0.72 and 0.86 and reaction stoichiometries, α, of 3.8 and 3.7 at 250 mM and 400 mM NaCl, respectively. *B*, when the Y-substrate was radiolabeled to monitor the release of the viral fragment (*open circles*), an additional competing hydrolysis reaction was detected at 2×10^{-5} s^{-1}, which quantitatively accounted for the missing amplitude observed for the disintegration reaction (*closed circles*). The *solid lines* represent the predicted time courses of disintegration for 0.5 μM DNA and 2.0 μM integrase at 250 mM NaCl with and without an additional exponential phase at 2×10^{-5} s^{-1}.

tion instead of disintegration. Thus, the amplitude observed in the active site titrations represented a fraction of integrase-substrate complex that underwent disintegration as opposed to hydrolysis, leading us to conclude that the measured reaction stoichiometry of four was accurately determined without further adjustments.

Atomic Force Microscopy Volume Determination—The reaction stoichiometry of four defined by the active site titrations, while necessary, is not sufficient to establish a tetrameric functional oligomeric state. To verify an active tetrameric structure, we determined the molecular weight of integrase complexes in the presence and absence of DNA by AFM volumetric analysis using the linear relationship between measured AFM volumes and molecular weights previously established for proteins ranging from 41 to 670 kDa (24, 25). To ensure the functional relevance of the particles imaged, depositions were made during the first turnover within 10 s of initiating the reaction.

A typical 1-μm^2 AFM image of integrase alone showed primarily particles with volumes consistent with monomers and dimers (Fig. 4*A*, *top*). By comparison, increased numbers of tetramer-sized particles were observed in images deposited in the presence of the Y-shaped substrate (Fig. 4*A*, *bottom*). Analysis of the integrated volumes for all particles imaged confirmed that in the absence of DNA, integrase appeared predominantly as monomers and dimers (Fig. 4*B*, *top*). In contrast, a new peak with a mean molecular volume of 154 ± 7.5 nm^3, corresponding to a calculated molecular weight of 138 kDa, became apparent and accounted for ~20% of the particles in the presence of DNA (Fig. 4*B*, *bottom*). When these population distributions were adjusted to more accurately reflect the number of integrase protomers subsumed within each volumetric subpopulation by taking into account the mass of each particle (Fig. 4*C*), we observed that the presence of substrate DNA induced nearly half of the integrase protomers analyzed to assemble into tetramers. Aggregates larger than tetramers, though visible, did not accumulate in sufficient numbers to segregate into discrete populations of a defined size, *e.g.* an octamer, and were therefore excluded from the statistical analysis. Additionally, the small number of these larger aggregates is inconsistent with the magnitude of productive complexes observed in the presteady-state burst.

The 138-kDa apparent mass observed was larger than expected for a tetramer of four 32-kDa subunits presumably due to the additional presence of the bound DNA. However, the apparent difference of 10 kDa underestimated the actual mass of the DNA. It is plausible that part of the volume contributed by the DNA may be topologically obscured within the concavity of the DNA binding site. Alternatively, the linear calibration curve determined for globular proteins is unlikely to yield accurate volume to mass conversion for DNA whose partial specific volume in aqueous solution can be considerably smaller than for proteins.

Hypothetical Structural Models of Integrase Tetramers—The structure of the full-length 32-kDa integrase protein is unknown. However, the central catalytic core domain (15–17) and all two-domain fragments consisting of the core plus either the C (18–20) or N terminus (21), from a variety of retroviral sources, form dimers in the crystal structures. Based on these structures, several dimer-of-dimers models have been proposed (20–22). Fig. 5A shows a recent model proposed based on the structure of the core plus N-terminal two-domain structure of HIV-1 integrase (21). In this model, a pair of inward-facing functional active sites is contributed by the two inner, or "proximal," protomers at the dimer-dimer interface. The two remaining outward-facing active sites of the two "distal" protomers are not used for catalysis (20–22). Coordinated processing of both ends of the viral DNA would therefore require concurrent binding of the two viral ends in active sites on both sides of the dimer-dimer interface (Fig. 5*A*).

Our results suggest that concerted integration may further require binding of the target DNA bridging the dimer-dimer interface (Fig. 5*B*). Although we cannot be certain of the molecular details of DNA binding in the absence of cocrystal structure, the observation that the Y-substrate, with only a single viral-end mimic, was able to induced active tetramer assembly would suggest significant contribution by the target DNA in mediating the dimer-dimer interaction. The calculated electrostatic potential at the surface of the proposed tetramer (Fig. 5*B*) shows that a ~30-Å wide, positively charged groove extends along this interface, suggesting that the assembly of the tetramer would require the juxtaposition of two positively charged surfaces. The neutralization of this like-charge repulsion by the binding of the negatively charged target DNA into this groove would greatly enhance the stability of the tetramer and may form the molecular basis for the observed DNA-induced assembly.

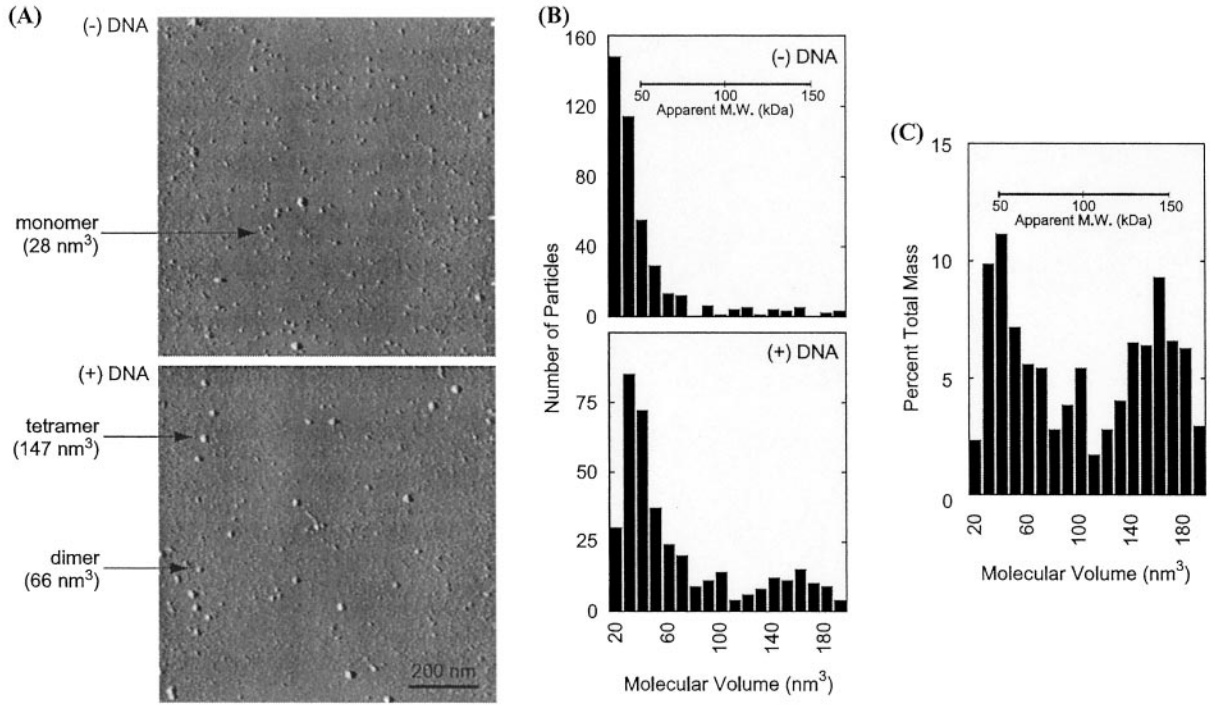

FIG. 4. *A*, AFM images of integrase deposited at 64 nM integrase in 150 mM NaCl showed mostly monomers and dimers with an occasional tetramer (*top*). This population was shifted in favor of dimers and tetramers in the presence of 80 nM substrate DNA (*bottom*). Excess DNA was used to disfavor the formation of tetramers. Images at higher integrase and NaCl concentrations also showed similar substrate-enhanced tetramerization. Images were created with the freeware program WSxM (www.nanotec.es). *B*, volume histograms of 405 and 381 particles analyzed in the absence (*top*) and presence (*bottom*) of substrate, respectively, showed a statistically significant increase in the tetramer population upon the addition of DNA. The *inset* axis represents the molecular volume to molecular weight conversion. *C*, when the histogram from *B* with substrate present was adjusted to reflect the mass of each particle, nearly half of the total integrase molecules were found in the tetrameric state.

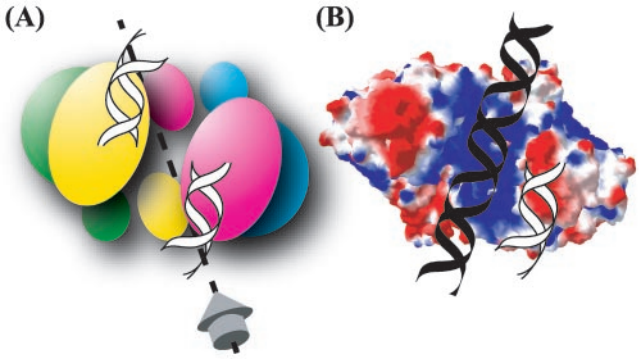

FIG. 5. *A*, the dimer-of-dimer tetramer proposed by Wang *et al.* (21) based on the structure of HIV-1 integrase1–212 (Protein Data Bank code 1K6Y) is schematically represented as a pair of crystallographic dimers (*green-yellow* and *blue-red*) using large and small ellipsoids to represent the core and N terminus domains, respectively. Viral DNA ends (*white ribbons*) are superimposed in the active sites of the two proximal protomers (*yellow* and *blue*). The *dashed line* indicates the plane of the dimer-dimer interface. *B*, the molecular surface of the tetramer is shown with positive and negative electrostatic potentials shown in *blue* and *red*, respectively. The image was created with DeepView/Swiss-PdbViewer (30). Products of the disintegration reaction from a Y-shaped substrate are superimposed on the tetramer guided by an active site and the positively charged central cleft, which is canted ~40° from the plane of the dimer-dimer interface. *Black* and *white ribbons* represent target and viral DNA, respectively. The neutralization of the positive charge at the dimer-dimer interface by the target DNA may provide the molecular basis for the observed DNA-induced tetramer assembly.

Relevance of the Disintegration Reaction—Despite being widely employed for assaying the activity of integrase and integrase mutants (8, 12–14), including that of the catalytic core domain constructs used in crystallographic studies (15–17, 27, 28), concerns persist that the disintegration reaction may not be mechanistically relevant. The skepticism arises in part from the observation that the catalytic core domain can catalyze the disintegration reaction but not the forward joining reaction, leading to the notion that the disintegration reaction might represent a less "stringent" measure of activity. While it may be more compelling to determine the reaction stoichiometry for the more obviously relevant processing or joining reactions, the results reported here with the disintegration reaction represent the first successful quantitative measure of a reaction stoichiometry using *any* integrase assay, because the propensity of the enzyme to aggregate has precluded the use of both the processing and the joining reaction in active site titrations (9, 10). Additionally, the reported weak disintegration activity of the ASV catalytic core (16) is > 100-fold slower than the competing, nonspecific hydrolysis reaction shown in Fig. 3*B* and at least 5 orders of magnitude slower than the disintegration activity reported here for the full-length enzyme (data not shown). This result, therefore, suggests that the disintegration reaction may not be as permissive as previously thought, at least for the ASV enzyme.

A more substantive concern regarding the use of the disintegration assay stems from the inclusion of only one viral-end mimic in the structural design of the Y-shaped substrate. As a result, our data do not directly rule out an octameric (dimer of tetramers) model (20–22) for the binding of two viral ends. However, as the minimum requisite set of active sites are present in a tetramer to bind both viral ends plus the target DNA, the available data likewise do not dictate any direct need to recruit additional active sites. In the absence of direct evidence for a higher order aggregate, we therefore favor the minimally sufficient tetrameric model. We note further that while the tetramer with a single Y-shaped substrate bound can accommodate the additional binding of a second viral end, the 30-Å wide groove of the tetramer is too narrow to permit the binding of a second Y-shaped substrate. Additionally, the complementary relation-

ship between the structure of this substrate and its ability to mediate functional tetramer assembly lends compelling support for the structural and functional relevance of the disintegration substrate in modeling the active-site architecture.

Implications for Structural Studies and Antiviral Design—Our ability to complete active site titrations suggests that the presence of target DNA in the disintegration substrate mitigated protein aggregation problems observed with other DNA substrates. Alternatively, the disintegration substrate conferred sufficient binding stability to maintain active complexes at the higher NaCl concentrations required to prevent aggregation. These results suggest potential benefits from using disintegration-like substrates, containing both target and viral DNA, in structural studies of the active integrase unit to promote tetramer formation as well as to minimize non-productive aggregation.

The observed substrate DNA- and metal cofactor-dependent oligomerization further suggests that the assembly of the active tetramer may be an integral and dynamic component of the catalytic pathway. The dynamic nature of the dimer-dimer interface should make it an ideal target for inhibitor design. The diketo acid family of inhibitors targeting the active site of integrase has recently been shown to inhibit the V(D)J recombinase, RAG1/2 (29), important for T- and B-cell development. Recently, we have independently characterized a novel RAG1/2-like "splicing" activity of ASV integrase that further suggests that any active-site directed inhibitor of integrase could similarly interfere with V(D)J recombination (9). If the substrate binding-induced assembly of an active tetramer lies along the kinetic pathway of catalysis, then inhibitors that disrupt the dimer-dimer interface may provide an enzyme-specific means of disrupting catalytic activity while avoiding possible adverse effects resulting from directly targeting the active site.

Acknowledgments—We thank Yong Yang for technical assistance in obtaining the AFM scans. All kinetic data were obtained in the laboratory of Dr. Isaac Wong by Dr. Kogan Bao. All AFM images were obtained in the laboratory of Dr. Dorothy Erie by Dr. Kogan Bao. and H. W. Additionally, we thank Drs. Daniel Herschlag and James Cole for critical readings of the manuscript.

REFERENCES

1. Grandgenett, D. P., and Mumm, S. R. (1990) *Cell* **60,** 3–4
2. Katz, R. A., and Skalka, A. M. (1994) *Annu. Rev. Biochem.* **63,** 133–173
3. Brown, P. O., Bowerman, B., Varmus, H. E., and Bishop, J. M. (1989) *Proc. Natl. Acad. Sci. U. S. A.* **86,** 2525–2529
4. Bushman, F. D., Fujiwara, T., and Craigie, R. (1990) *Science* **249,** 1555–1558
5. Fujiwara, T., and Mizuuchi, K. (1988) *Cell* **54,** 497–504
6. Katz, R. A., Merkel, G., Kulkosky, J., Leis, J., and Skalka, A. M. (1990) *Cell* **63,** 87–95
7. Kukolj, G., and Skalka, A. M. (1995) *Genes Dev.* **9,** 2556–2567
8. Chow, S. A. (1997) *Methods* **12,** 306–317
9. Bao, K. K., Skalka, A. M., and Wong, I. (2002) *J. Biol. Chem.* **277,** 12089–12098
10. Bao, K. K., Skalka, A. M., and Wong, I. (2002) *J. Biol. Chem.* **277,** 12099–12108
11. Chow, S. A., Vincent, K. A., Ellison, V., and Brown, P. O. (1992) *Science* **255,** 723–726
12. Vincent, K. A., Ellison, V., Chow, S. A., and Brown, P. O. (1993) *J. Virol.* **67,** 425–437
13. Mazumder, A., Wang, S., Neamati, N., Nicklaus, M., Sunder, S., Chen, J., Milne, G. W., Rice, W. G., Burke, T. R., Jr., and Pommier, Y. (1996) *J. Med. Chem.* **39,** 2472–2481
14. Puras-Lutzke, R. A., Eppens, N. A., Weber, P. A., Houghten, R. A., and Plasterk, R. H. (1995) *Proc. Natl. Acad. Sci. U. S. A.* **92,** 11456–11460
15. Dyda, F., Hickman, A. B., Jenkins, T. M., Engelman, A., Craigie, R., and Davies, D. R. (1994) *Science* **266,** 1981–1986
16. Bujacz, G., Jaskolski, M., Alexandratos, J., Wlodawer, A., Merkel, G., Katz, R. A., and Skalka, A. M. (1995) *J. Mol. Biol.* **253,** 333–346
17. Goldgur, Y., Dyda, F., Hickman, A. B., Jenkins, T. M., Craigie, R., and Davies, D. R. (1998) *Proc. Natl. Acad. Sci. U. S. A.* **95,** 9150–9154
18. Chen, Z., Yan, Y., Munshi, S., Li, Y., Zugay-Murphy, J., Xu, B., Witmer, M., Felock, P., Wolfe, A., Sardana, V., Emini, E. A., Hazuda, D., and Kuo, L. C. (2000) *J. Mol. Biol.* **296,** 521–533
19. Chen, J. C., Krucinski, J., Miercke, L. J., Finer-Moore, J. S., Tang, A. H., Leavitt, A. D., and Stroud, R. M. (2000) *Proc. Natl. Acad. Sci. U. S. A.* **97,** 8233–8238
20. Yang, Z. N., Mueser, T. C., Bushman, F. D., and Hyde, C. C. (2000) *J. Mol. Biol.* **296,** 535–548
21. Wang, J. Y., Ling, H., Yang, W., and Craigie, R. (2001) *EMBO J.* **20,** 7333–7343
22. Heuer, T. S., and Brown, P. O. (1998) *Biochemistry* **37,** 6667–6678
23. Craigie, R. (2001) *J. Biol. Chem.* **276,** 23213–23216
24. Ratcliff, G. C., and Erie, D. A. (2001) *J. Am. Chem. Soc.* **123,** 5632–5635
25. Xue, Y., Ratcliff, G. C., Wang, H., Davis-Searles, P. R., Gray, M. D., Erie, D. A., and Redinbo, M. R. (2002) *Biochemistry* **41,** 2901–2912
26. Asante-Appiah, E., and Skalka, A. M. (1997) *J. Biol. Chem.* **272,** 16196–16205
27. Jenkins, T. M., Hickman, A. B., Dyda, F., Ghirlando, R., Davies, D. R., and Craigie, R. (1995) *Proc. Natl. Acad. Sci. U. S. A.* **92,** 6057–6061
28. Engelman, A., Hickman, A. B., and Craigie, R. (1994) *J. Virol.* **68,** 5911–5917
29. Melek, M., Jones, J. M., O'Dea, M. H., Pais, G., Burke, T. R., Jr., Pommier, Y., Neamati, N., and Gellert, M. (2002) *Proc. Natl. Acad. Sci. U. S. A.* **99,** 134–137
30. Guex, N., and Peitsch, M. C. (1997) *Electrophoresis* **18,** 2714–2723